arXiv:1412.7466v1 [math.NA] 23 Dec 2014

A fast and robust solver for the scattering from a layered periodic structure containing multi-particle inclusions

Jun Lai*, Motoki Kobayashi†, and Alex Barnett‡

December 24, 2014

Abstract

We present a solver for plane wave scattering from a periodic dielectric grating with a large number M of inclusions lying in each period of its middle layer. Such composite material geometries have a growing role in modern photonic devices and solar cells. The high-order scheme is based on boundary integral equations, and achieves many digits of accuracy with ease. The usual way to periodize the integral equation—via the quasi-periodic Green's function—fails at Wood's anomalies. We instead use the free-space Green's kernel for the near field, add auxiliary basis functions for the far field, and enforce periodicity in an expanded linear system; this is robust for all parameters. Inverting the periodic and layer unknowns, we are left with a square linear system involving only the inclusion scattering coefficients. Preconditioning by the single-inclusion scattering matrix, this is solved iteratively in $\mathcal{O}(M)$ time using a fast matrix-vector product. Numerical experiments show that a diffraction grating containing $M = 1000$ inclusions per period can be solved to 9-digit accuracy in under 5 minutes on a laptop.

Keywords: fast solver, periodic scattering, multi-particle scattering, layered medium, diffraction

1 Introduction

The modeling and design of periodic dielectric structures plays a central role in modern optics. Tools such as diffraction gratings, photonic crystals, meta-materials, plasmonics, and other micro-scale structures, are becoming key to efficient devices, including lasers, sensors, anti-reflective surfaces and absorbers [21], and solar cells [3]. For instance, in thin-film solar cell design [44, 29] the use of periodic structures, and nanoparticle inclusions, in ordered or disordered composites, enhances absorption. One then seeks a grating structure with a specific arrangement of inclusions that maximizes absorption. Other optimization problems include the design of photonic crystal lenses [35]. Related is the inverse problem of inferring a structure from measurements [37, 5]. Such tasks demand a large number of solutions of the direct (forward) scattering problem. Similar periodic and multi-particle wave scattering problems arise in acoustics and elastodynamics, and in general whenever a *super-cell* is used to approximate the response of a random composite material (e.g. [36]). Such considerations have spurred the development of efficient methods for solving Helmholtz and Maxwell frequency-domain boundary value problems in periodic geometries [21, 7, 14, 9, 10, 23, 13, 18]. High accuracy can be challenging to achieve due to guided modes, resonances, and extreme parameter sensitivity.

*Courant Institute of Mathematical Sciences, New York University, NY 10012. Email: *lai@cims.nyu.edu*

†Courant Institute of Mathematical Sciences, New York University, NY 10012. Email: *motokia.kobayashi@gmail.com*

‡Department of Mathematics, Dartmouth College, Hanover, NH 03755. Email: *ahb@math.dartmouth.edu*

Therefore, in this paper we consider the monochromatic scattering from a layered periodic structure containing a large number M of inclusions ("particles") at given locations, as in a (generalized) photonic crystal. As shown in Fig. 1, the structure is periodic in the x direction, layered in the y direction and invariant along the z direction. Because of the two-dimensional (2D) geometry, there exist two fundamental polarizations in the electromagnetic scattering: transverse magnetic (TM) where the magnetic field is transverse to the (x, y) plane, and transverse electric (TE) where the electric field is transverse to the (x, y) plane. We will focus on TM polarization, noting that our technique applies to TE polarization without any essential difficulty.

The grating scattering problem has been mathematically very well studied. It has been proved that for an arbitrary periodic dielectric and incident angle the problem has a unique solution for all frequencies with the possible exception of a countable set of resonances (singular frequencies [11]) at which the solution is not unique. Such physical resonances are not to be confused with *Wood's anomalies* (for the definition see the next section), which are frequencies where at least one of the Bragg diffraction orders points along the grating, i.e. in the x direction. A Wood's anomaly does not prevent the solution from being unique, although it does cause arbitrarily large sensitivity with respect to the incident wave angle or frequency [33], and also causes problems with certain integral equation methods [10]. One of the advantages of our scheme is that it is applicable and accurate at or near Wood's anomalies, without any modifications.

There exists a wide range of numerical methods for periodic diffraction, including boundary integral equations [2, 14, 10, 23, 13, 18], finite element methods [4, 8], Fourier expansion based methods [38], and continuation methods [15]. In the time domain, the finite difference scheme has been discussed in [26]. The advantages of the integral approach over finite elements and finite differences are that it reduces the dimension by one (vastly reducing the number of unknowns), and achieves high-order accuracy with appropriate surface quadratures. However, the resulting linear system is often dense, making a naive matrix-vector product expensive when the number of unknowns is large. In this paper, we will reduce this cost via the fast multipole method (FMM) [24].

More specifically, we propose an integral approach based on the free space Green's function; this bypasses the considerable complexities of computing the periodic Green's function [30, 13]. We split the representation of the scattered field in the grating structure into near field and far field components. The near field is represented by standard free-space Helmholtz single- and double-layer potentials on the material interfaces, while the far field is taken care by a *local expansion* (Fourier–Bessel or J expansion) whose coefficients are fixed by enforcing the periodic boundary condition explicitly in the linear system. This builds upon recent ideas of the last author and co-workers [9, 10, 18].

Solving for discretized layer densities on each of the M inclusion boundaries would introduce an unnecessarily large number of unknowns. Hence, following [22, 32], we precompute the inclusion *scattering matrices*, then treat the set of outgoing scattering coefficients as a reduced set of unknowns. When particles are sub-wavelength, and not extremely close to each other, this is highly accurate with only 20 or so unknowns per particle [32]. The full rectangular linear system then couples these to the grating interface densities and periodizing J-expansion coefficients. By eliminating the last two (via a Schur complement and pseudoinverse) we are left with a square linear system for the particle scattering coefficients, which we precondition with a block-diagonal matrix and then solve via GMRES with FMM acceleration, with effort scaling linearly in M. The result is a robust, efficient, high-order accurate solver that we expect to be useful for design and optimization problems for periodic photonic devices.

The outline of the paper is as follows. Section 2 gives the mathematical formulation of the periodic problem. Section 3 proposes the integral approach for the scattering from a periodic structure without particle inclusions, based on the free space Green's function. Section 4 reviews classical multi-particle scattering and discusses the evaluation of the scattering matrix. The quasi-periodizing scheme combining all the above techniques is given in Section 5, and numerical experiments are shown in Section 6. We draw conclusions in Section 7.

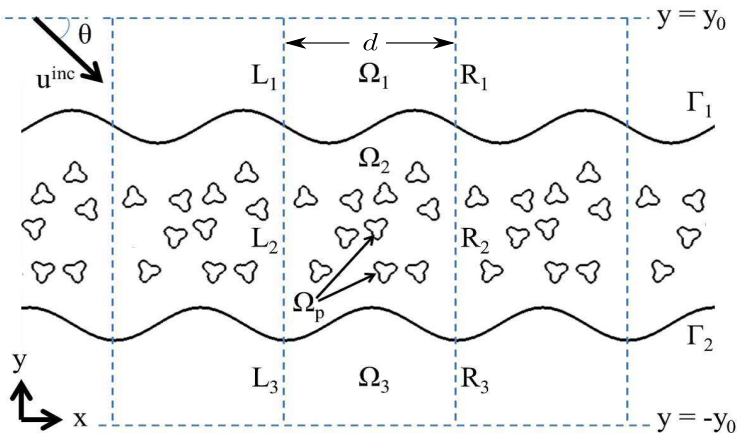

Figure 1: A 2D grating scattering geometry: a plane wave incident on a three-layered periodic structure with periodicity d. A large number of identical dielectric obstacles are embedded in the middle layer. We use Ω_p to denote the set of all these particles and Ω_p^j to denote the jth particle. The vertical dotted lines indicate the unit cell walls $x = d/2 \pm ld$, $l = 1, 2, 3, \cdots$, while the top and bottom dotted lines indicate the fictitious boundaries at $\pm y_0$. The three layers are denoted by Ω_1, Ω_2 and Ω_3.

2 Problem formulation

Consider the plane-wave incident time harmonic scattering (with time dependence $e^{-i\omega t}$) from a 2D periodic (or grating) structure with period d. As shown in Figure 1, the unit cell $\Omega = [-d/2, d/2] \times \mathbb{R}$ consists of three layers, denoted by Ω_1, Ω_2 and Ω_3. Let Γ_1 and Γ_2 denote the two smooth interfaces separating the layers. The left and right boundaries of Ω_j are denoted by L_j and R_j, $j = 1, 2, 3$. Assume the permittivity ε is given as ε_1, ε_2 and ε_3 in the three layers respectively. A large number M of particles, collectively denoted by Ω_p, with the same permittivity ε_p, are located inside Ω_2. The permeability μ is assumed to be constant everywhere.

For TM polarization, in which case the total electric field is $E(x, y) = (0, 0, u)$, the full time harmonic Maxwell equations

$$\begin{cases} \nabla \times E &= i\omega\mu H \\ \nabla \times H &= -i\omega\varepsilon E \end{cases}$$

are reduced to the Helmholtz equation:

$$\Delta u + k(\mathbf{x})^2 u = 0 \ , \tag{1}$$

where $\mathbf{x} := (x, y)$, and where the wavenumber k takes one of four values,

$$k(\mathbf{x}) = \begin{cases} k_1 := \omega\sqrt{\mu\varepsilon_1}, & \mathbf{x} \in \Omega_1 \\ k_2 := \omega\sqrt{\mu\varepsilon_2}, & \mathbf{x} \in \Omega_2 \backslash \overline{\Omega_p} \\ k_3 := \omega\sqrt{\mu\varepsilon_3}, & \mathbf{x} \in \Omega_3 \\ k_p := \omega\sqrt{\mu\varepsilon_p}, & \mathbf{x} \in \Omega_p \end{cases} \tag{2}$$

In the usual setting of scattering theory, the full wave is $u = u^{\text{inc}} + u^{\text{sc}}$, where u^{inc} is the incident wave and u^{sc} is the resulting wave scattered from the periodic structure. The incident wave is a plane wave $u^{\text{inc}}(x, y) = e^{ik_1 \cos\theta x + ik_1 \sin\theta y}$ in Ω_1, and $u^{\text{inc}} = 0$ elsewhere, with θ the incident angle.

Since the wave is propagating in different layers, the continuity condition along various interfaces in TM polarization with constant permeability is:

$$[u] = 0 \ , \qquad \left[\frac{\partial u}{\partial n}\right] = 0 \ , \tag{3}$$

where $[\cdot]$ denotes the jump of a function across the interface, $\partial/\partial n$ is the normal derivative, and u is the total field in each layer [20].

We use the term *quasi-periodic* if a function (such as u) satisfies

$$u(x+d, y) = e^{i\kappa d} u(x, y) \qquad \text{for all } (x, y) \ , \tag{4}$$

where $\kappa = k_1 \cos\theta$ is the incident horizontal wavevector. The factor

$$\alpha := e^{i\kappa d}$$

is the Bloch phase associated with translation by one period. Since u^{inc} is quasi-periodic, we seek a scattered wave with this same symmetry, hence (4) also holds for the full wave [41]. Restricting to a single unit cell, with left and right walls L and R respectively, we have matching conditions

$$\alpha u_L - u_R = 0 \tag{5}$$

$$\alpha \left.\frac{\partial u}{\partial n}\right|_L - \left.\frac{\partial u}{\partial n}\right|_R = 0 \tag{6}$$

which are in fact equivalent to (4) [11, Sec. 3].

Finally, u^{sc} must satisfy a radiation condition. Let y_0 be sufficiently large such that Ω_2 lies between the lines $\Gamma_u := \{y = y_0\}$ and $\Gamma_d := \{y = -y_0\}$ (see Figure 1). Define $\kappa_n = \kappa + 2\pi n/d$, $n \in \mathbb{Z}$, and $k_{j,n} = +\sqrt{k_j^2 - \kappa_n^2}$, where $j = 1, 3$ and the sign of the square-root is taken as positive real or positive imaginary. Then the plane wave with wavevector $(\kappa_n, k_{j,n})$ is quasi-periodic for each integer n, and satisfies the Helmholtz equation at frequency ω. The radiation condition on u^{sc} is expressed by uniformly convergent *outgoing or decaying* Rayleigh–Bloch expansions:

$$u^{\text{sc}}(x, y) = \sum_{n\in\mathbb{Z}} c_n e^{i\kappa_n x} e^{ik_{1,n}(y-y0)}, \qquad \text{for } y > y_0, x \in \mathbb{R}, \tag{7}$$

$$u^{\text{sc}}(x, y) = \sum_{n\in\mathbb{Z}} d_n e^{i\kappa_n x} e^{ik_{3,n}(-y-y0)}, \qquad \text{for } y < -y_0, x \in \mathbb{R}. \tag{8}$$

The complex coefficients c_n, d_n, for n such that $|\kappa_n| \le k_j$ (propagating waves), are the Bragg diffraction amplitudes at the grating orders. For all other n these give evanescent components which do not contribute to the far field. A Wood's anomaly occurs if, for some n, $\kappa_n = k_1$, thus $k_{1,n} = 0$ (upper half-space), or if $\kappa_n = k_3$ thus $k_{3,n} = 0$ (lower half-space). The radiation conditions ensure that u^{sc} is outgoing except at a Wood's anomaly, when the nth Rayleigh–Bloch mode in (7) or (8) is constant in y (a horizontally traveling plane wave). It is also possible to have a double Wood's anomaly, when $\kappa_n = \kappa_m = k_1$ for a pair of integers n, m.

The following theorem [4, 6, 11] describes the well-posedness of the boundary value problem.

Theorem 2.1. *Fixing an incident angle θ, there exists a unique solution u to* (1)–(3) *and* (5)–(8) *for all but a discrete set of ω.*

Henceforth we will assume parameter values (θ, ω) for which the solution is unique.

To summarize, we are interested in the solution of (1) together with the continuity condition (3), the unit-cell quasi-periodicity (5)–(6), and the radiation condition (7)–(8) satisfied by u^{sc}. In the next section we discuss the solution for the layered periodic structure without inclusions, via the integral equation approach.

Remark 1. From now on we slightly abuse the notation Ω_1, Ω_2 and Ω_3 introduced, by replacing them by their truncated versions. In other words, Ω_1 has boundaries L_1, Γ_1, R_1, and Γ_u, while Ω_3 has boundaries L_3, Γ_d, R_3, and Γ_2. The unit cell will refer to $\Omega = \Omega_1 \cup \Omega_2 \cup \Omega_3 = [-d/2, d/2] \times [-y_0, y_0]$. The artificial upper and lower boundaries Γ_u and Γ_d are also called transparent boundaries in some literature [7].

3 Robust solution for empty periodic layered structure

The standard approach to convert a non-periodic integral equation formulation into the correct periodic one is to use the quasi-periodic Green's function [34], defined at wavenumber k_j as

$$G^{\text{qp}}_{k_j}(\mathbf{x}, \mathbf{y}) := \sum_{l \in \mathbb{Z}} \alpha^l G_{k_j}(\mathbf{x}, \mathbf{y} + (ld, 0)) \ , \tag{9}$$

where $\mathbf{x} \in \Omega_j$ is the target and $\mathbf{y} \in \Omega_j$ the source point, and G_k is the free space Green's function at wavenumber k, i.e. $G_k(\mathbf{x}, \mathbf{y}) = \frac{i}{4} H_0^{(1)}(k\|\mathbf{x} - \mathbf{y}\|)$, where $H_0^{(1)}$ is the outgoing Hankel function of order zero, and $\|\cdot\|$ is the Euclidean norm. (9) is well-defined away from Wood's anomalies, and has been successfully applied in many grating problems [2, 14, 23, 41]. However, it has two major practical drawbacks: i) it is expensive to evaluate (requiring either series acceleration, or lattice sums [34]), and ii) it blows up (with an inverse-square-root singularity) at Wood's anomalies, causing a purely numerical breakdown in the solution of a what remains a well-posed problem. The key idea is that (9) can be rewritten as

$$G^{\text{qp}}_{k_j}(\mathbf{x}, \mathbf{y}) = \sum_{l=-P}^{P} \alpha^l G_{k_j}(\mathbf{x}, \mathbf{y} + (ld, 0)) + \sum_{n \in \mathbb{Z}} a_n J_n(k_j \|\mathbf{x} - \mathbf{x_0}\|) e^{in\theta_{\mathbf{x}-\mathbf{x}_0}} \tag{10}$$

where P is a positive integer, $\mathbf{x}_0 \in \Omega_j$ is a fixed origin, $\theta_{\mathbf{x}}$ is the angle of a vector $\mathbf{x}$, J_n is the Bessel function of order n, and the *lattice sum* coefficients $\{a_n\}$ can be found by Graf's addition theorem [40, 10.23(ii)]. The second term accounts for the smooth field due to the infinite set of far sources $l < -P$ and $l > P$ from (9). The $2P + 1$ direct terms account for the near field.

Remark 2. The sum in (10) converges (and exponentially fast) if and only if the target is closer to the origin than the nearest "far" source, i.e. $\|\mathbf{x} - \mathbf{x}_0\| < \min_{l \in \mathbb{Z}, l \notin [-P,P]} \|\mathbf{y} + (ld, 0) - \mathbf{x}_0\|$. This geometric condition is satisfied with $P = 1$ for all $\mathbf{x}, \mathbf{y} \in \Omega_j$ if the region Ω_j is not much taller than d, and $\mathbf{x}_0$ is placed near the center of Ω_j. Thus, we will use $P = 1$ in our numerical experiments. However, if Ω_j is much taller than d (high aspect ratio), then P needs to be increased to guarantee uniform convergence.

Using this idea in the scattering setting we represent the scattered field in the first layer as,

$$u_1^{\text{sc}}(\mathbf{x}) = \sum_{l=-P}^{P} \alpha^l \mathbf{S}^{k_1}_{\Gamma_1^l} \sigma_1 + \sum_{l=-P}^{P} \alpha^l \mathbf{D}^{k_1}_{\Gamma_1^l} \mu_1 + \sum_{n \in \mathbb{Z}} a_n^{(1)} J_n(k_1 \|\mathbf{x} - \mathbf{x}_1\|) e^{in\theta_{\mathbf{x}-\mathbf{x}_1}} \ , \qquad \mathbf{x} \in \Omega_1 \tag{11}$$

where Γ_1^l is the lth periodic translation of $\Gamma_1^0 \in \Omega$, i.e. $\cup_{l \in \mathbb{Z}} \Gamma_1^l = \Gamma_1$, σ_1 and μ_1 are unknown periodic density functions defined on the interface Γ_1, and $\mathbf{x}_1 \in \Omega_1$ is choice of origin. The coefficients $\{a_n^{(1)}\}$ are now unknown and need to be determined by the boundary conditions. $\mathbf{S}$ and $\mathbf{D}$ are the usual single- and double-layer potentials [19], which we may define living on a general interface Γ at wavenumber k by,

$$(\mathbf{S}^k_\Gamma \sigma)(\mathbf{x}) = \int_\Gamma G_k(\mathbf{x}, \mathbf{y}) \sigma(\mathbf{y}) ds_{\mathbf{y}} \tag{12}$$

$$(\mathbf{D}^k_\Gamma \mu)(\mathbf{x}) = \int_\Gamma \frac{\partial G_k(\mathbf{x}, \mathbf{y})}{\partial n(\mathbf{y})} \mu(\mathbf{y}) ds_{\mathbf{y}} \tag{13}$$

These representations satisfy the Helmholtz equation at wavenumber k in $\mathbb{R}^2\backslash\Gamma$; thus the representation (11) satisfies the relevant Helmholtz equation in Ω_1. When restricted to target points on Γ these give the boundary integral operators $S^k_{\Gamma,\Gamma}$ (which is weakly singular), and $D^k_{\Gamma,\Gamma}$ (which is continous for Γ smooth, and is to be interpreted in the principal value sense). Here and in what follows, the notation S_{Γ_i,Γ_j} means the operator from source curve Γ_j to target curve Γ_i. We will also need the operators corresponding to the target normal derivatives on Γ,

$$(N^k_{\Gamma,\Gamma}\sigma)(\mathbf{x}) = \int_\Gamma \frac{\partial G_k(\mathbf{x},\mathbf{y})}{\partial n(\mathbf{x})}\sigma(\mathbf{y})ds_\mathbf{y} \ , \qquad (T^k_{\Gamma,\Gamma}\mu)(\mathbf{x}) = \int_\Gamma \frac{\partial^2 G_k(\mathbf{x},\mathbf{y})}{\partial n(\mathbf{x})\partial n(\mathbf{y})}\mu(\mathbf{y})ds_\mathbf{y} \ , \quad \mathbf{x}\in\Gamma \ . \tag{14}$$

The operator $T^k_{\Gamma,\Gamma}$ is *hypersingular* and defined in the Hadamard finite part sense. The books [19, 20] give further details.

We also need the *jump relations* that relate the limiting values of (12)–(13) to the actions of the above boundary integral operators. Let $u^\pm(\mathbf{x}) := \lim_{h\to 0^+} u(\mathbf{x}+hn(\mathbf{x}))$ and $u^\pm_n(\mathbf{x}) := \lim_{h\to 0^+} n(\mathbf{x})\cdot\nabla u(\mathbf{x}+hn(\mathbf{x}))$ be the limiting values and normal derivatives approaching $\mathbf{x}\in\Gamma$ from the positive $(+)$ or negative $(-)$ side. Then for all continuous densities σ and μ,

$$(\mathbf{S}^k_\Gamma\sigma)^\pm = S^k_{\Gamma,\Gamma}\sigma \tag{15}$$
$$(\mathbf{S}^k_\Gamma\sigma)^\pm_n = (-\tfrac{1}{2}+N^k_{\Gamma,\Gamma})\sigma \tag{16}$$
$$(\mathbf{D}^k_\Gamma\mu)^\pm = (\tfrac{1}{2}+D^k_{\Gamma,\Gamma})\mu \tag{17}$$
$$(\mathbf{D}^k_\Gamma\mu)^\pm_n = T^k_{\Gamma,\Gamma}\mu \tag{18}$$

Thus the single-layer potential is continuous for all $\mathbf{x}$, whereas the double-layer is generally discontinuous across Γ.

Turning to the third layer Ω_3, we similarly represent the scattered field $u^{\rm sc}$ using layer potentials on Γ_2,

$$u^{\rm sc}_3(\mathbf{x}) = \sum_{l=-P}^{P}\alpha^l\mathbf{S}^{k_3}_{\Gamma_2^l}\sigma_2 + \sum_{l=-P}^{P}\alpha^l\mathbf{D}^{k_3}_{\Gamma_2^l}\mu_2 + \sum_{n\in\mathbb{Z}} a^{(3)}_n J_n(k_3\|\mathbf{x}-\mathbf{x}_3\|)e^{in\theta_{\mathbf{x}-\mathbf{x}_3}}, \qquad \mathbf{x}\in\Omega_3 \tag{19}$$

where $\mathbf{x}_3\in\Omega_3$. The scattered field in the second layer has contribution from both Γ_1 and Γ_2, thus

$$\begin{aligned} u^{\rm sc}_2(\mathbf{x}) = &\sum_{l=-P}^{P}\alpha^l\mathbf{S}^{k_2}_{\Gamma_1^l}\sigma_1 + \sum_{l=-P}^{P}\alpha^l\mathbf{D}^{k_2}_{\Gamma_1^l}\mu_1 \\ &+ \sum_{l=-P}^{P}\alpha^l\mathbf{S}^{k_2}_{\Gamma_2^l}\sigma_2 + \sum_{l=-P}^{P}\alpha^l\mathbf{D}^{k_2}_{\Gamma_2^l}\mu_2 + \sum_{n\in\mathbb{Z}} a^{(2)}_n J_n(k_2\|\mathbf{x}-\mathbf{x}_2\|)e^{in\theta_{\mathbf{x}-\mathbf{x}_2}}, \quad \mathbf{x}\in\Omega_2 \end{aligned} \tag{20}$$

where $\mathbf{x}_2\in\Omega_2$.

To determine the unknown densities σ_1, σ_2, μ_1, μ_2 and the coefficients $a^{(1)}_n$, $a^{(2)}_n$ and $a^{(3)}_n$, we enforce the following boundary conditions according to (3) and (5)–(8).

- On Γ^0_1 and Γ^0_2, the continuity condition (3) is imposed, giving,

$$\begin{cases} (u^{\rm sc}_1 - u^{\rm sc}_2)|_{\Gamma^0_1} = -u^{\rm inc}|_{\Gamma^0_1} \\ \left(\frac{\partial u^{\rm sc}_1}{\partial n} - \frac{\partial u^{\rm sc}_2}{\partial n}\right)\Big|_{\Gamma^0_1} = -\frac{\partial u^{\rm inc}}{\partial n}\Big|_{\Gamma^0_1} \\ (u^{\rm sc}_2 - u^{\rm sc}_3)|_{\Gamma^0_2} = 0 \\ \left(\frac{\partial u^{\rm sc}_2}{\partial n} - \frac{\partial u^{\rm sc}_3}{\partial n}\right)\Big|_{\Gamma^0_2} = 0 \end{cases} \tag{21}$$

  Note that since the representation of $u^{\rm sc}$ in the three layers involves layer potentials, the limits must be taken from the appropriate side of Γ_1 and Γ_2 using jump relations (15)–(18).

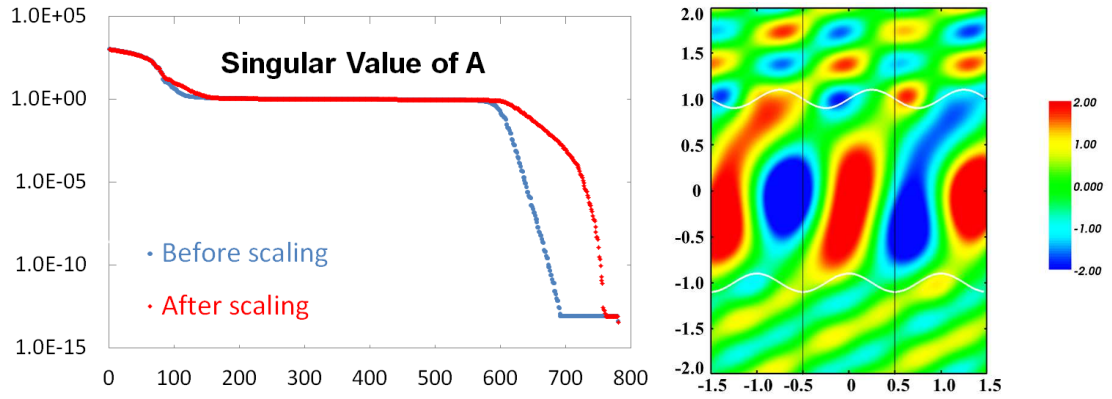

Figure 2: Scattering from a periodic structure without inclusions, with $k_1 = 10$, $k_2 = 5$, $k_3 = 10$ and $d = 1$. The interfaces are Γ_1 given by the graph $y = 1 + 0.1\sin(2\pi x)$, and Γ_2 the graph $y = -1 + 0.1\cos(2\pi x)$. (a) The singular value spectrum σ_j of matrix $\mathcal{A}$, vs index j: original matrix (blue dots), vs after rescaling the columns of the blocks in $\mathcal{A}$ corresponding to J expansions (red dots). (b) Real part of the scattered field computed to 13-digit accuracy.

- On L_j and R_j, where $j = 1, 2, 3$, the quasi-periodicity condition (4) is imposed:

$$\begin{cases} \alpha u_j^{\rm sc}|_{L_j} - u_j^{\rm sc}|_{R_j} = 0 \\ \alpha \dfrac{\partial u_j^{\rm sc}}{\partial n}\Big|_{L_j} - \dfrac{\partial u_j^{\rm sc}}{\partial n}\Big|_{R_j} = 0 \end{cases} \tag{22}$$

  The left hand sides (phased differences) is sometimes known as the *discrepancy* [10].

- On the parts of the artificial boundaries Γ_u and Γ_d lying in the unit cell Ω (denote this part of the boundary by Γ_u^0 and Γ_d^0), the radiation conditions (7) and (8) are imposed for values and normal derivatives:

$$\begin{cases} (u_1^{\rm sc} - \sum_{n\in\mathbb{Z}} c_n e^{i\kappa_n x})|_{\Gamma_u^0} = 0 \\ \left(\dfrac{\partial u_1^{\rm sc}}{\partial n} - \sum_{n\in\mathbb{Z}} i c_n k_{1,n} e^{i\kappa_n x}\right)\Big|_{\Gamma_u^0} = 0 \\ (u_3^{\rm sc} - \sum_{n\in\mathbb{Z}} d_n e^{i\kappa_n x})|_{\Gamma_d^0} = 0 \\ \left(\dfrac{\partial u_1^{\rm sc}}{\partial n} + \sum_{n\in\mathbb{Z}} i d_n k_{3,n} e^{i\kappa_n x}\right)\Big|_{\Gamma_d^0} = 0 \end{cases} \tag{23}$$

Substituting the representations (11), (19) and (20) into conditions (21)–(23), one reaches a system of coupled integral and functional equations that can only be solved numerically, which means the interfaces must be discretized, and the infinite series truncated. The J expansions are truncated up to order Q, i.e. they retain $2Q + 1$ terms. The centers of the J expansion $\mathbf{x}_1$, $\mathbf{x}_2$ and $\mathbf{x}_3$ should be located roughly in the centers of the domains Ω_1, Ω_2 and Ω_3. We discretize the four interfaces Γ_1, Γ_2, Γ_u and Γ_d using equally spaced points (Γ_1 and Γ_2 are discretized through equally-spaced nodes in their parametrizations). The left and right boundary L_j and R_j are discretized by Gauss–Legendre nodes. The singular integrals involved in the layer potentials are discretized via the Nyström method [27], with 16th-order Alpert quadrature corrections [1]. A phase correction is applied to account for the Bloch phase factors when the parameter "wraps" around the end of the open curves Γ_1^0 or Γ_2^0. The standard application of quadrature rules, and the use of the Alpert scheme, is described in [18, Sec. 2.5] (see the smooth case only).

In the end, stacking as block rows the equations (21), (22) and (23), the linear system for the discretized layered periodic structure without particle inclusions (the "empty" structure) takes the form,

$$\begin{bmatrix} A_{11} & A_{12} & A_{1m} & 0 & 0 & 0 & 0 \\ A_{21} & A_{22} & A_{2m} & 0 & 0 & 0 & 0 \\ A_{w1} & A_{w2} & A_{wm} & 0 & 0 & 0 & 0 \\ A_{wu1} & 0 & 0 & A_{wuu} & 0 & 0 & 0 \\ 0 & A_{wd2} & 0 & 0 & 0 & A_{wdd} & 0 \\ A_{u1} & 0 & 0 & A_{uu} & A_{ur} & 0 & 0 \\ 0 & A_{d2} & 0 & 0 & 0 & A_{dd} & A_{dr} \end{bmatrix} \begin{bmatrix} \nu_1 \\ \nu_2 \\ \mathbf{a}^{(2)} \\ \mathbf{a}^{(1)} \\ \mathbf{a}^{(3)} \\ \mathbf{c} \\ \mathbf{d} \end{bmatrix} = \begin{bmatrix} v^i \\ 0 \\ 0 \\ 0 \\ 0 \\ 0 \\ 0 \end{bmatrix} \tag{24}$$

Here the right-hand side vector has the form

$$f := [v^i, 0, 0, 0, 0, 0, 0]^T \text{ with } v^i := [-u^{\text{inc}}|_{\Gamma_1^0},\ -\partial u^{\text{inc}}/\partial n|_{\Gamma_1^0}]. \tag{25}$$

The unknown coefficient vector, which we will call $\vec{\alpha}$, stacks the discretizations of the paired densities $\nu_j := [\mu_j; \sigma_j]$ for interfaces $j = 1, 2$, the coefficient vectors $\mathbf{a}^{(j)}$ for the J-expansions in layers $j = 1, 2, 3$, and the Rayleigh–Bloch coefficient vectors $\mathbf{c}$ and $\mathbf{d}$ from (7)–(8). We may then summarize (24) by

$$\mathcal{A}\vec{\alpha} = f\ .$$

We now describe the matrix blocks in $\mathcal{A}$ (for readability we do not give formulae for every single block, trusting that their construction is unambiguous from the above; for more detail in a related scheme see [18]). Each block maps unknowns to values and normal derivatives at target nodes, or their phased differences between left and right walls. Matrix entries involve either free-space Green's functions between source and target nodes, or J or Rayleigh–Bloch expansions at target nodes.

- A_{11} and A_{22}: Nyström self-interaction matrices for Γ_1^0 and Γ_2^0 respectively, including the phased summation over $2P+1$ source near neighbors. For instance,

$$A_{11} = \begin{bmatrix} I + \sum_{l=-P}^{P} \alpha^l (D^{k_1}_{\Gamma_1^0,\Gamma_1^l} - D^{k_2}_{\Gamma_1^0,\Gamma_1^l}) & \sum_{l=-P}^{P} \alpha^l (T^{k_1}_{\Gamma_1^0,\Gamma_1^l} - T^{k_2}_{\Gamma_1^0,\Gamma_1^l}) \\ \sum_{l=-P}^{P} \alpha^l (S^{k_1}_{\Gamma_1^0,\Gamma_1^l} - S^{k_2}_{\Gamma_1^0,\Gamma_1^l}) & -I + \sum_{l=-P}^{P} \alpha^l (N^{k_1}_{\Gamma_1^0,\Gamma_1^l} - N^{k_2}_{\Gamma_1^0,\Gamma_1^l}) \end{bmatrix} \tag{26}$$

  (where here and below, the Nyström discretizations of the various operators are implied), maps $[\mu_1; \sigma_1]$ at the N quadrature nodes on Γ_1^0 to the field jumps $[u_1^{\text{sc}} - u_2^{\text{sc}}; \partial u_1^{\text{sc}}/\partial n - \partial u_2^{\text{sc}}/\partial n]$ at these same N nodes. I indicates the N-by-N identity matrix. All terms (after subtractions) are compact apart from the identities, meaning that this subsystem is of Fredholm second kind. Recall that the identities originate in the jump relations (15)–(18). This BIE scheme for dielectric interfaces is due in the electromagnetic case to Müller [39], and the acoustic case to Kress–Roach [28] and Rokhlin [42].

- A_{21}, A_{12}: interaction of ($2P+1$ summed) source densities on Γ_1 with value and normal derivatives on Γ_2, and vice versa, at wavenumber k_2.

- A_{1m}, A_{2m}: values and normal derivatives of the middle-layer J-expansion on Γ_1^0, Γ_2^0.

- A_{w1}, A_{w2}, and A_{wm}: phased differences of values and normal derivatives between the left and right walls L_2 and R_2 in (22) (case $j = 2$), due to the layer potentials on Γ_1, Γ_2, and the middle-layer J-expansion respectively. A_{wu1}, A_{wuu}: phased differences for upper walls (case $j = 1$) due to layer potentials on Γ_1 and the upper J-expansion. A_{wd2}, A_{wdd}: phased differences for lower walls (case $j = 3$) due to layer potentials on Γ_2 and the lower J-expansion.

- A_{u1}, A_{uu} (A_{d2}, A_{dd}): values and normal derivatives of the layer potentials on Γ_1 (Γ_2), and the upper (lower) J-expansions, evaluated on the upper boundary Γ_u^0 (lower boundary Γ_d^0).

- A_{ur}, A_{dr}: values and normal derivatives of the Rayleigh–Bloch expansions on the upper and lower boundaries Γ_u^0, Γ_d^0 respectively.

Remark 3. The lower-right 5×5 block of $\mathcal{A}$ in (24) involves only the effect of the auxiliary periodizing degrees of freedom (J and Rayleigh–Bloch expansions) on the auxiliary matching conditions (discrepancies and radiation conditions). In related work this block is given the symbol Q [10, 18].

The matrix $\mathcal{A}$ is generally rectangular, depending on the specific numbers of discretization nodes. Although the upper-left 2×2 block of $\mathcal{A}$ is a square system coming from a Fredholm second kind system of BIEs, the other blocks involve J-expansions evaluated on interfaces and walls, which make $\mathcal{A}$ as a whole exponentially ill-conditioned. Figure 2(a) shows the singular values of $\mathcal{A}$: there are many singular values clustered around 10^{-14}, although the situation is alleviated a little by rescaling the columns that correspond to the J-expansions (also shown). However, such ill-conditioning is not an obstacle as long as the system is consistent: since $\mathcal{A}$ is not too large (of typical size 10^3 for k_j corresponding to up to several wavelengths across one period d), we may use direct dense linear algebra for a small-norm least-squares solution. We use the `mldivide` command in MATLAB. Figure 2(b) shows the resulting real part of the scattered field with a total flux error (whose definition will be given in section 6) of 10^{-13}.

4 Multi-particle scattering

Multi-particle scattering in free space has been discussed extensively in [22, 32, 31], with applications including climatology, remote sensing, and design of composite materials. Recently, we have developed a fast solver for finding the field scattered from a large number of particles located in a layered medium, by combining the Sommerfeld integral and multiple scattering theory. Here we briefly review the method introduced in [32], and then combine it with the periodic grating. See [32, 22] for more details. Note that our approach can be seen as a simple version of a reduced basis method [16].

4.1 Scattering matrix of a single particle

Consider for now a dielectric inclusion with wavenumber $k_p = \omega\sqrt{\epsilon_p \mu}$ surrounded by uniform dielectric with $k_2 = \omega\sqrt{\epsilon_2 \mu}$. When the inclusion is a disk of radius R centered at the origin, it is well known that the solution can be represented using separation of variables, with

$$u(r,\theta) = \sum_{n=-\infty}^{\infty} \alpha_n J_n(k_p r) e^{in\theta} \tag{27}$$

in the interior, and scattered wave

$$u^{\text{sc}}(r,\theta) = \sum_{n=-\infty}^{\infty} \beta_n H_n^{(1)}(k_2 r) e^{in\theta} \tag{28}$$

in the exterior. Here, (r,θ) are the polar coordinates of a point in the plane, and $H_n^{(1)}(r)$ is the Hankel function of the first kind of order n.

Definition 4.1. The mapping between the incoming coefficients $\{\alpha_n\}$ and outgoing coefficients $\{\beta_l\}$ is referred as the *scattering matrix*. It will be denoted by S, with matrix elements s_{ln}.

For a single disk, the scattering matrix S is diagonal and is easily found analytically [19]; this is not true for an arbitrary inclusion shape. We instead seek a solution via BIE, using the Müller–Kress–Roach–Rokhlin scheme from the previous section. Suppose that the inclusion Ω_p has boundary

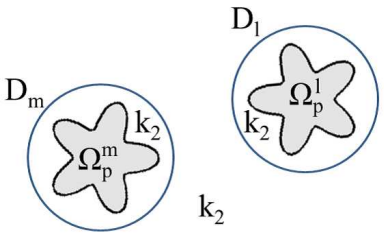

Figure 3: Two inclusions and their enclosing disks. The scattering matrix S_j for each inclusion Ω_p^j with wavenumber k_p is defined as the map from an incoming field on D_j to the corresponding outgoing field.

$\partial\Omega_p$ and is enclosed by a disk D centered at the origin. Given the incident wave u^{inc} and the boundary conditions (3), the exterior scattered field u^{sc} and the field u within Ω_p have the following representations [19]:

$$u^s = \mathbf{S}^{k_2}\sigma + \mathbf{D}^{k_2}\mu, \qquad \text{for } \mathbf{x} \in \Omega_p^c, \tag{29}$$

$$u = \mathbf{S}^{k_p}\sigma + \mathbf{D}^{k_p}\mu, \qquad \text{for } \mathbf{x} \in \Omega_p. \tag{30}$$

Here σ and μ are unknown single- and double-layer densities on $\partial\Omega_p$, and, in this section without ambiguity we drop the subscripts $\partial\Omega_p$. Enforcing the interface conditions (3) and taking appropriate limits using jump relations (15)–(18) yields a system of Fredholm integral equations of the second kind:

$$\mu + (S^{k_2} - S^{k_p})\sigma + (D^{k_2} - D^{k_p})\mu = -u^{\text{inc}}, \tag{31}$$

$$-\sigma + (N^{k_2} - N^{k_p})\sigma + (T^{k_2} - T^{k_p})\mu = -\frac{\partial u^{\text{inc}}}{\partial n}. \tag{32}$$

Let σ_n and μ_n denote the solution to (31)–(32) for $u^{\text{inc}}(r,\theta) = J_n(kr)e^{in\theta}$. We may then precompute the scattering matrix elements s_{ln} as the multipole expansion coefficients (truncated up to $2p+1$ terms)

$$u^{\text{sc}}(r,\theta) \approx \sum_{l=-p}^{p} s_{ln} H_l^{(1)}(k_2 r) e^{il\theta}\,, \tag{33}$$

from the densities σ_n and μ_n via Graf's addition theorem, giving the standard formula [43, 17]

$$s_{ln} = \int_{\partial\Omega_p} J_l(k_2\|\mathbf{y}\|)e^{-il\theta_{\mathbf{y}}}\,\sigma_n(\mathbf{y}) + n(\mathbf{y})\cdot\nabla[J_l(k_2\|\mathbf{y}\|)e^{-il\theta_{\mathbf{y}}}]\mu_n(\mathbf{y})\,ds_{\mathbf{y}}\,. \tag{34}$$

4.2 Multiple inclusions

Suppose now that we have M inclusions $\Omega_p^1, \ldots, \Omega_p^M$ that are identical up to translation and rotation, and are well separated in the sense that each inclusion Ω_p^m lies within a disk D_m of radius R such that the disks are not overlapping (see Fig. 3). The incident wave for the mth inclusion may now be expanded as

$$u^{\text{inc}}(\mathbf{x}) \approx \sum_{n=-p}^{p} a_n^{(m)} J_n(k_2 r_m) e^{in\theta_m} \tag{35}$$

where (r_m, θ_m) are defined to be the polar coordinates of $\mathbf{x}$ relative to the center of D_m. We will denote by $\vec{\alpha}^m$ the set of $2p+1$ incoming coefficients, and by $\vec{\beta}^m$ the $2p+1$ outgoing coefficients, for the mth particle. Thus

$$\vec{\beta}^m = S_p^{(m)} \vec{\alpha}^m, \qquad \text{for } m = 1, \ldots, M. \tag{36}$$

where $S_p^{(m)}$ denotes the truncated $(2p+1) \times (2p+1)$ scattering matrix acting on the truncated expansion about the center of the mth particle. If the particles were only translated, we would have $S_p^{(m)} = S_p$ for all m, where S_p is the truncated scattering matrix from the previous section with elements s_{ln}. We allow general rotations of particles; rotation of the mth particle by angle ϕ introduces phase factors, so $(S_p^{(m)})_{ln} = e^{i\phi(l-n)} s_{ln}$.

Multi-particle scattering has a key difference from single particle scattering, namely that the incoming field experienced by each particle consists of two parts: the (applied) incident field u^{inc}, and the contribution to the scattered field u^{sc} from all of the *other* particles. We denote by T^{jm} the *translation operator* (or M2L in FMM language [43]) that maps the outgoing coefficient vector $\vec{\beta}^m := \{\beta_n^m\}_{n=-p}^p$ from particle m to their contribution to the local expansion coefficients $\vec{\alpha}^j$ centered at particle j. With this operator in place, the incoming coefficients $\vec{\alpha}^m$ for the mth particle are

$$\vec{\alpha}^m = \vec{a}^m + \sum_{\substack{j=1 \\ j \neq m}}^{M} T^{jm} \vec{\beta}^j, \tag{37}$$

where $\vec{a}^m$ is the (truncated) local expansion (35) of the incident wave u^{inc} relative to particle m.

Combining (36) and (37), one can easily eliminate the incoming coefficients $\vec{\alpha}^m$ to obtain the following linear system that only involves the outgoing coefficients:

$$\left(\mathcal{S}^{-1} - \mathcal{T}\right) \begin{bmatrix} \vec{\beta}^1 \\ \vec{\beta}^2 \\ \vdots \\ \vec{\beta}^M \end{bmatrix} = \begin{bmatrix} \vec{a}^1 \\ \vec{a}^2 \\ \vdots \\ \vec{a}^M \end{bmatrix}, \tag{38}$$

where

$$\mathcal{S} := \begin{bmatrix} S_p^{(1)} & & & \\ & S_p^{(2)} & & \\ & & \ddots & \\ & & & S_p^{(M)} \end{bmatrix}, \quad \mathcal{T} := \begin{bmatrix} 0 & T^{21} & \cdots & T^{M1} \\ T^{12} & 0 & \cdots & T^{M2} \\ \vdots & \vdots & \ddots & \vdots \\ T^{1M} & T^{2M} & \cdots & 0 \end{bmatrix}.$$

The system (38) can be solved iteratively, using GMRES. Since each translation operator T^{nm} is dense, a naive matrix-vector product requires $\mathcal{O}(M^2(2p+1)^2)$ operations, where p is the order of the truncated expansion. The cost can be reduced to $\mathcal{O}(M(2p+1)^2)$ work by FMM acceleration, for which we refer the reader to [43, 17]. Furthermore, there exists an effective preconditioner for the system (38). Left-multiplying by the block diagonal matrix $\mathcal{S}$ results in the preconditioned system matrix $I - \mathcal{S}\mathcal{T}$. This significantly reduces the number of iterations.

The advantage of using the one-particle scattering matrices $S_p^{(m)}$ over boundary integral equations is clear: the number of degrees of freedom per inclusion is only $2p+1$ rather than the number of nodes needed to discretize the domain boundaries $\partial\Omega_p^m$. For complicated inclusions, this permits a vast reduction in the number of degrees of freedom required, forming the basis for the so-called FMPS method [22]. Moreover, the block-diagonal preconditioned multiple scattering equations are much better conditioned than the BIE (31)–(32), while FMM acceleration is particularly fast in this setting.

Remark 4. It is straightforward to extend the method to more than one type of particles as long as the assumption that the enclosed circles are well separated still holds. The additional cost is simply the bookkeeping for the different scattering matrices.

5 Multi-particle scattering in the periodic layered medium

We now combine the schemes of the previous two sections. The field in the middle layer is the periodic layered contribution u_2^{sc} from (20), plus the scattered field from the M inclusions and, cruicially, their $2P$ neighboring near-field phased copies. We need the notation (r_m^l, θ_m^l) for polar coordinates relative to the origin of the mth particle translated by $(ld, 0)$. Then,

$$u_2(\mathbf{x}) = u_2^{\text{sc}}(\mathbf{x}) + \sum_{l=-P}^{P} \alpha^l \sum_{j=1}^{M} \sum_{n=-p}^{p} \beta_n^m H_n^{(1)}(k_2 r_m^l) e^{in\theta_m^l}, \quad \mathbf{x} \in \Omega_2 \backslash \Omega_p \ . \tag{39}$$

It only remains to set up the interactions between the layered periodic structure and the inclusion structure. We denote the translation matrix mapping layer densities and the middle-layer J expansion to the incoming coefficients of all particles by $\mathcal{B}$, and the translation matrix mapping (phased summed) outgoing particle multipole coefficients to data on the layers and walls by $\mathcal{C}$. Adhering to the ordering of unknowns and conditions in (24), one can show that they have the forms (since the particles interact only with the middle layer),

$$\mathcal{B} = \begin{bmatrix} B_{p1} & B_{p2} & B_{pm} & 0 & 0 & 0 & 0 \end{bmatrix}, \tag{40}$$

$$\mathcal{C} = \begin{bmatrix} C_{1p} & C_{2p} & C_{wp} & 0 & 0 & 0 & 0 \end{bmatrix}^T, \tag{41}$$

where here $[\cdot]^T$ denotes the blockwise transpose. B_{p1}, B_{p2} and B_{pm} map layer densities on Γ_1, Γ_2 and the J expansion to the incoming coefficients of the particles. C_{1p}, C_{2p}, and C_{wp} map the outgoing coefficients from particles to the values and normal derivatives on interfaces Γ_1, Γ_2 and the discrepancy from L_2 to R_2.

It is easy to construct the elements in C_{1p}, C_{2p}, and C_{wp} by direct evaluation of multipole expansions. Note that C_{wp} involves *cancellations* which mean that only particle-wall interactions over distances greater than d survive, as discussed in Remark 6.

To obtain the elements in B_{p1}, B_{p2} and B_{pm}, one again uses Graf's addition theorem. In particular, the translation submatrix B_{pm} that maps the coefficients from one J expansion to another J expansion (the local-to-local or L2L operator in the FMM) is constructed through the following lemma.

Lemma 5.1 ([43]). *Let disk m be centered at $\mathbf{x}_m$ and let disk l be centered at $\mathbf{x}_l$. Then the local expansion*

$$\sum_{n=-\infty}^{\infty} \gamma_n^m J_n(k_2 r_m) e^{in\theta_m} \tag{42}$$

induces a field on disk l of the form

$$u = \sum_{n'=-\infty}^{\infty} \alpha_{n'}^l J_{n'}(k_2 r_l) e^{in'(\theta_l - \pi)} \tag{43}$$

where

$$\alpha_{n'}^l = \sum_{n=-\infty}^{\infty} e^{i(n-n')\theta_{\mathbf{x}_m - \mathbf{x}_l}} \gamma_{n-n'}^m J_n(k_2 \|\mathbf{x_m} - \mathbf{x_l}\|).$$

Let us denote by $\vec{\beta} := \{\vec{\beta}^m\}_{m=1}^M$ the multipole coefficients for all M particles in Ω_2. Combining the matrices (24), (38), (40) and (41), we obtain the final system:

$$\begin{bmatrix} \mathcal{A} & \mathcal{C} \\ \mathcal{B} & \mathcal{D} \end{bmatrix} \begin{bmatrix} \vec{\alpha} \\ \vec{\beta} \end{bmatrix} = \begin{bmatrix} f \\ 0 \end{bmatrix}, \tag{44}$$

where $\mathcal{D} = \mathcal{S}^{-1} - \mathcal{T}$, as in (38), and f is the right-hand side vector (25).

Since (44) is a rectangular ill-conditioned matrix, we cannot easily solve this whole system iteratively. However, we now present a Schur complement scheme to generate a smaller, well-conditioned square linear system for which an iterative solution is efficient. Since $\mathcal{A}$ has size of order 10^3 in both dimensions, it is much smaller than $\mathcal{D}$, and we can eliminate the unknowns $\vec{\alpha}$ via $\vec{\alpha} = \mathcal{A}^+(f - C\vec{\beta})$, where $\mathcal{A}^+$ is the pseudoinverse of $\mathcal{A}$. We precompute $\mathcal{A} = U\Sigma V^*$, the singular value decomposition of $\mathcal{A}$, where the singular values are σ_j. Then to apply $\mathcal{A}^+$ to an arbitrary vector g we use matrix-vector multiplies,

$$\mathcal{A}^+ g = V\Sigma^+(Ug) \ , \tag{45}$$

where Σ^+ has diagonal elements $\min[1/\sigma_j, 1/\epsilon]$. The regularization parameter is fixed at $\epsilon = 10^{-10}$; its precise choice is not crucial, but empirically it is best chosen to be roughly the desired solution accuracy.

Remark 5. Forming the matrix $\mathcal{A}^+$ then multiplying it against a vector g is dangerous, since it can cause large and unnecessary round-off error. Rather, (45) should be used since it is backward stable and hence introduces the minimum possible round-off error.

Substitution for $\vec{\alpha}$ into the full linear system gives the Schur complement

$$(\mathcal{D} - \mathcal{B}\mathcal{A}^+\mathcal{C})\vec{\beta} = -\mathcal{B}\mathcal{A}^+ f \ , \tag{46}$$

a relatively well-conditioned square system involving only unknowns $\vec{\beta}$. The new system matrix has a physical interpretation: it is the particle-particle interaction matrix using the layered-medium quasi-periodic Green's function, where $\mathcal{B}\mathcal{A}^+\mathcal{C}$ is a low-rank update to $\mathcal{D}$. We can use GMRES on this system, using FMM acceleration to apply $\mathcal{D}$, $\mathcal{B}$ and $\mathcal{C}$, and the factorization (45) to apply $\mathcal{A}^+$. The cost (for moderate frequencies) is then an optimal $\mathcal{O}(M)$ per iteration.

As we mentioned in section 4, left-preconditioning via $\mathcal{S}$ can improve the conditioning of the system. We therefore end up solving the following,

$$(I - \mathcal{S}\mathcal{T} - \mathcal{S}\mathcal{B}\mathcal{A}^+\mathcal{C})\vec{\beta} = -\mathcal{S}\mathcal{B}\mathcal{A}^+ f \ , \tag{47}$$

with the same cost per iteration as (46) (the small dense multiplications by S_p being cheap), but fewer needed iterations.

6 Numerical experiments

In this section, we demonstrate the performance of our algorithm with three examples. For simplicity, we use a single class of particles, parametrized by

$$\begin{cases} x &= (a_1 + a_2\cos(a_3 t))\cos(t), \\ y &= (a_1 + a_2\cos(a_3 t))\sin(t), \end{cases} \quad \text{for } 0 \le t < 2\pi. \tag{48}$$

Particles with more complicated boundaries do not introduce any essential difficulty in our scheme, except that the precomputation of the scattering matrix is a little more involved, particularly if corners are present [12, 25]. However, regardless of complexity, the size of the needed scattering matrix $(2p+1)$ depends only on the particle size in wavelengths and the closeness of nearby particles. Given a fixed a_1, a_2 and a_3, multiple copies of the inclusion are randomly distributed in the central layer of the medium with random orientations.

To provide an independent test of accuracy, we check flux conservation. If all wavenumbers k_1, k_2, k_3 and k_p are real, the Rayleigh–Bloch coefficients satisfy the identity (eg see [33])

$$\sum_{k_{1,n}>0} k_{1,n}|c_i|^2 + \sum_{k_{3,n}>0} k_{3,n}|d_i|^2 = k_1 \sin\theta \tag{49}$$

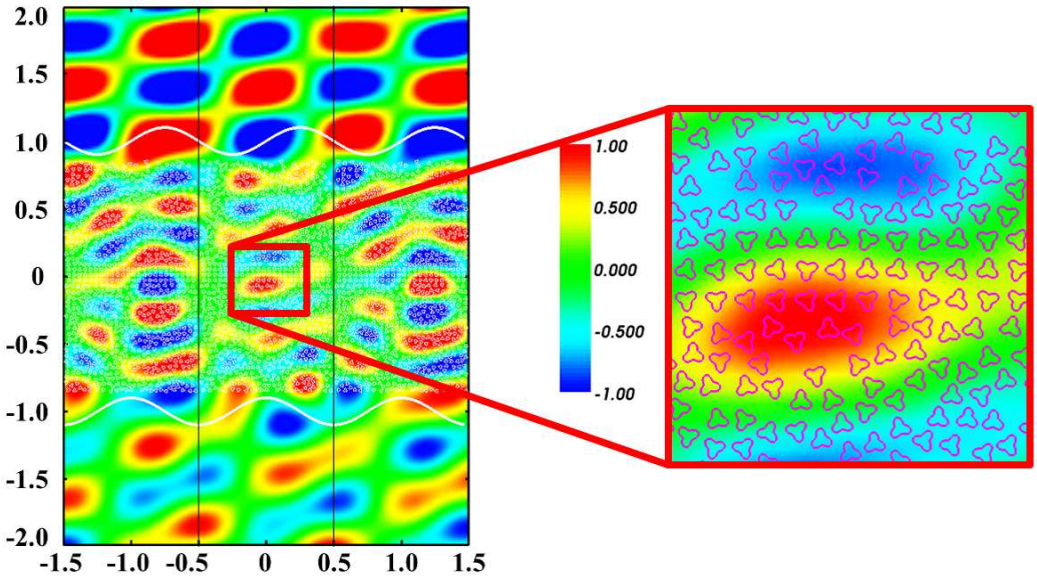

Figure 4: Real part of the total field with 1000 dielectric inclusions randomly distributed in a three-layered medium (see Example 1). The wavenumber for each particle is $k_p = 30$ and the wavenumbers for the three layers are $k_1 = 10$, $k_2 = 8$, $k_3 = 10$. The diameter of each particle is approximately 0.2 wavelengths at the wavenumber k_p.

In other words, the outgoing energy flux must equal the incoming energy flux. *Flux error* then refers to the size of the difference between the left and right sides.

Throughout all the numerical examples, the period is $d = 1$, and the near-field summation is fixed at $P = 1$ (i.e. three terms in the near-field sum). In the first two examples the interfaces Γ_1 and Γ_2 are given by the graphs $y = 1 + 0.1\sin(2\pi x)$ and $y = -1 + 0.2\cos(2\pi x)$ respectively.

Assume there is a modest distance between the inclusions Ω_p and the interfaces Γ_1 and Γ_2, say, at least 0.5 wavelengths in terms of the wavenumber k_2. Under this assumption, we may discretize Γ_1 and Γ_2 with $N = 120$ nodes each, equally spaced in x, which is sufficient to achieve 12 digits of accuracy with the periodized Alpert's quadrature for modest wavenumbers k_1, k_2 and k_3. The two artificial boundaries Γ_u and Γ_d are discretized equally in x with 50 points each. We use $2Q+1 = 73$ terms for the J expansions in each layer, and 41 Rayleigh–Bloch modes in each vertical direction. Based on these discretizations, $\mathcal{A}$ has size 1020×781.

All computations are carried out using a 2.3GHz Intel Core i5 laptop, with 4GB RAM.

6.1 Example 1: scattering from large numbers of inclusions

In our first example, we consider distributions of $M = 100$, 500 and 1000 inclusions with wavenumber $k_p = 30$, by assuming the incident angle is away from any Wood's anomaly, and the boundaries of the inclusions do not touch the wall L_2 or R_2. (Both restrictions will be removed, in our second and third examples, respectively.) The thickness of the central layer is fixed by the length of L_2 and R_2, given by $l = 2.0$. The size of each inclusion is therefore determined by the amount. Assume $a_3 = 3$ in Eq. (48). We let $a_1 = 0.0309$, $a_2 = 0.0103$ for $M = 100$, and $a_1 = 0.0154$, $a_2 = 0.00514$ for $M = 500$, and $a_1 = 0.0111$, $a_2 = 0.0037$ for $M = 1000$. To obtain the scattering matrix S_p with $p = 10$, we solve the integral Eqs. (31) and (32) by discretizing the boundary of the particle with $N = 300$ equispaced points. We assume the wavenumbers of the layered medium are given by $k_1 = 10$, $k_2 = 8$ and $k_3 = 10$. The incident angle is set to be $\theta = -\arccos(1.0-2\pi/10.0)+0.1 \approx -1.089976736488571$,

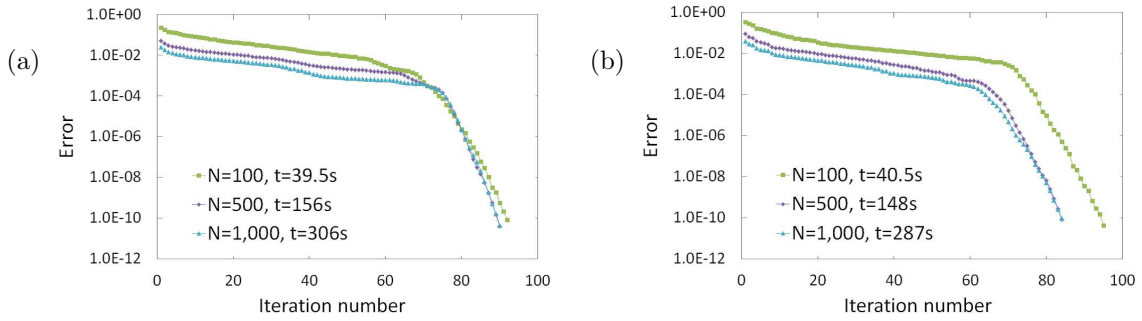

Figure 5: Convergence behavior of GMRES and the CPU time required for various numbers of periodized inclusions embedded in either (a) homogeneous medium or (b) a three-layered periodic medium, for Example 1. For (a), we set $k_1 = k_2 = k_3 = 10$ and for (b), we set $k_1 = 10$, $k_2 = 8$, $k_3 = 10$.

Number of particles	flux error, homogeneous case	flux error, three-layer case
100	1.05e-9	2.22e-10
500	4.03e-10	2.35e-10
$1,000$	1.59e-9	1.14e-9

Table 1: Flux error for various numbers of inclusions embedded in either (a) homogeneous medium or (b) a three layered medium, for Example 1.

which is not a Wood's anomaly for $k_1 = 10$, but is quite close to one. Results are presented in Figs. 4, 5 and Table 1.

Figure 4 shows the total field in the case $M = 1000$. Disordered propagation due to the random inclusions is apparent. The total number of unknowns in $\vec{\beta}$ is 21000, although if nodes on the particles were used it would be much higher. It requires 287s to achieve 9 digits of accuracy. Figure 5 shows the convergence behavior of GMRES as the number of inclusions is increased, and the total CPU times. In Fig. 5(a), we also study the convergence rate when the background is homogeneous, by setting the material parameters to be the same for the three layers ($k_1 = k_2 = k_3 = 10$). No obvious discrepancy in terms of the number of iterations has been observed, which suggests that the multiple scattering is dominated by the inclusions. Table 1 shows flux error in the cases above. In all cases we exceed 9 digits of accuracy.

Number of particles	number of iterations	GMRES error	CPU time (sec.)	Flux error
100	97	7.61e-11	41.2	1.03e-9
500	91	4.24e-11	156	3.21e-10
$1,000$	90	5.83e-11	307	2.48e-9

Table 2: Convergence behavior of GMRES, the CPU time required and flux error for various numbers of inclusions embedded in a three layered medium (see Example 2.)

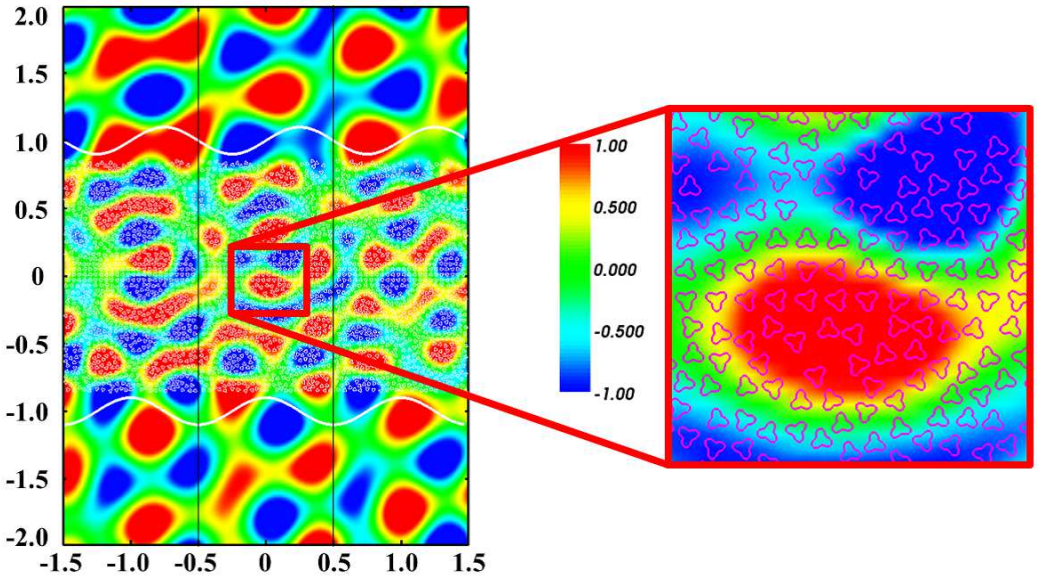

Figure 6: Real part of the total field when 1000 dielectric inclusions with $k_p = 30$ are randomly embedded in a three-layered medium with $k_1 = 10$, $k_2 = 8$ and $k_3 = 10$, as in Fig. 5. This is Example 2: the angle of the incident wave is at a Wood's anomaly.

k_2	number of iterations	GMRES error	CPU time (sec.)	Flux error
1	13	9.68e-11	18.0	8.54e-10
10	15	1.39e-11	18.9	7.52e-11
20	43	4.55e-11	26.6	4.38e-10
30	83	5.12e-11	37.8	1.02e-8

Table 3: Convergence behavior of GMRES, the CPU time required and flux error for 100 inclusions embedded in the central layer, where k_2 is allowed to vary from 1 to 30 (see Example 3).

6.2 Example 2: scattering from large numbers of inclusions at a Wood's anomaly

In our second example, we consider the same scattering as above except the change of incident angle. In particular, we let $\theta = -\arccos(1.0 - 2\pi/10.0) \approx -1.189976736488571$, which is a Wood's anomaly for $k_1 = 10$. Thus the classical quasi-periodic Green's function for the upper layer does not exist. However, our scheme is still able to obtain 10 digits of accuracy as shown in Fig. 6 and Table 2. The flux error suggests at least 9 digits of accuracy in all cases. The number of GMRES iterations and CPU times are almost the same as in Example 1.

6.3 Example 3: scattering from inclusions intersecting with unit cell walls

In our last example, we consider the scattering from 100 smoothed pentagons ($a_3 = 5$) with $k_p = 8$. In particular, we allow some of the inclusions intersect the wall L_2 and R_2, as shown in Fig. 7. We set the thickness of the central layer to be $l = 2.0$, and define parameters $a_1 = 0.0309$, $a_2 = 0.0103$ in Eq. (48). The boundary of the inclusion is discretized by $N = 300$ equispaced points and the scattering matrix S_p is truncated up to $p = 10$. The interfaces Γ_1 and Γ_2 are given by the graphs

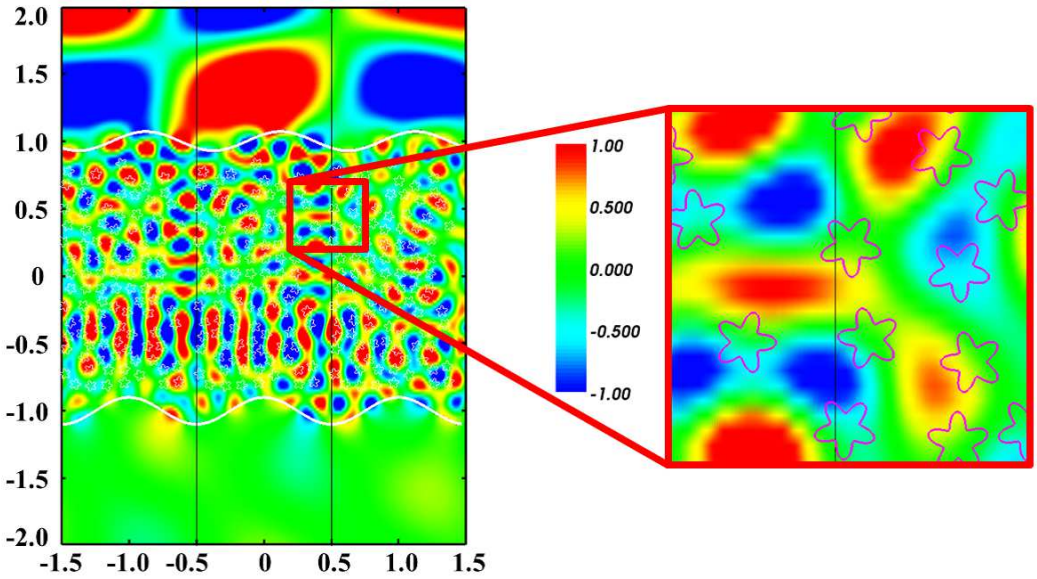

Figure 7: Real part of the total field with 100 dielectric inclusions, some of which touch the walls L_2 or R_2, randomly distributed in a three-layered medium (see Example 3). The wavenumber for each particle is $k_p = 8$, and the wavenumbers for the three layers are $k_1 = 5$, $k_2 = 30$ and $k_3 = 5$. Each inclusion is a smoothed five-pointed star, approximately 0.4 wavelengths in size for k_2.

$y = 1 + 0.05\sin(2\pi x) + 0.05\cos(2\pi x)$ and $y = -1 + 0.1\cos(2\pi x)$ respectively. The incident angle is set to be $\theta = -\arccos(1.0 - 2\pi/10.0) + 0.1$, which is the same as example 1.

Remark 6. Careful readers might think that our method should fail in this case, since the multipole expansion for each inclusion is only valid outside the disk that encloses the inclusion, yet some target nodes on the walls lie inside these disks. However, it turns out our scheme is still valid, by design, due to cancellation in the C_{wp} block due to translational symmetry: whatever field induced by $\Omega_p \in \Omega_2$ to L_2, it is equal to the field induced by Ω_p in the right copy of Ω_2 to R_2 up to the Bloch phase. Once the subtraction is made in Eq. (22), the two cancel each other. Thus the only effects of particle multipole expansions on the discrepancy between walls L_2 and R_2 are at a distance of around Pd or more. The walls are "invisible" to the particles in this scheme. This is discussed more explicitly in [10, Sec. 3.1] and [18, Sec. 2.3].

The above observation has been confirmed by the numerical tests, as shown in Fig. 7 and Table 3.

Figure 7 shows the total field in the case $k_2 = 30$. We can see smooth field distortion due to the inclusions, even though some of the inclusions intersect the walls L_2 and R_2. In Table 3, we test higher-contrast materials: the wavenumber in the middle layer varies from 1 to 30 for the three-layered medium. In all cases, we can get 10 digits of accuracy of GMRES and at least 8 digits accuracy has been guaranteed in terms of flux error.

7 Conclusion

We have demonstrated an efficient new scheme to solve the quasi-periodic boundary value problem arising when a time-harmonic plane wave is incident on a layered periodic structure containing a large number of inclusions, as occurs in various composites and solar cell designs. The method is based entirely on free-space Green's functions, using an expanded linear system to enforce quasi-periodicity

and radiation conditions explicitly. This avoids expensive computations of the quasi-periodic Green's function, yet is robust at all scattering parameters including Wood's anomalies (where the latter fails to exist). We have shown high accuracies even at Wood's anomalies, and with inclusions intersecting unit cell walls.

For the scattering between multiple inclusions, we introduce the scattering matrix for each inclusion and use it as a block-diagonal precondtioner, which greatly improves the conditioning of multi-particle scattering system. We also apply the FMM to accelerate the translation operator between the different structures. In the end, the system is solved iteratively by GMRES, scaling optimally (linearly) in M the number of inclusions, at fixed frequency. This claim of $\mathcal{O}(M)$ scaling holds only if the number of iterations is independent of M; however, our numerical tests suggest that any growth with M is very weak in our setting (see Fig. 5). Multi-particle systems with tens of thousands of unknowns are solved to around 9-digit accuracy on a laptop in a few minutes.

There are several possible extensions that we leave for future work. The method can easily be adapted to TE polarization, to complex permittivities, and to non-smooth inclusions. If higher aspect ratio unit cell regions (i.e. heights much bigger than the period) are needed, P can be increased, although this slows down the FMM which applies the large $\mathcal{D}$ matrix block. High aspect ratios could instead be handled by replacing the (intrinsically isotropic) J-expansions with proxy nodes as in [18], on oval curves. Our scheme naturally generalizes to bi-periodic structures in 3D, with the matrix $\mathcal{A}$ still directly invertible (with size of order 10^4) at low frequencies. Other future work includes a rigorous error analysis of the scheme.

8 Acknowledgments

The authors would like to thank Leslie Greengard for several useful discussions which greatly improved this paper.

References

[1] B. K. Alpert. Hybrid Gauss-trapezoidal quadrature rules. *SIAM J. Sci. Comput.*, 20:1551–1584, 1999.

[2] T. Arens, S. N. Chandler-Wilde, and J. A. DeSanto. On integral equation and least squares methods for scattering by diffraction gratings. *Commun. Comput. Phys.*, 1:1010–42, 2006.

[3] H. A. Atwater and A. Polman. Plasmonics for improved photovoltaic devices. *Nature Materials*, 9(3):205–213, 2010.

[4] G. Bao. Finite element approximation of time harmonic waves in periodic structures. *SIAM Journal on Numerical Analysis*, 32(4):1155–1169, 1995.

[5] G. Bao, T. Cui, and P. Li. Inverse diffraction grating of Maxwell's equations in biperiodic structures. *Opt. Express*, 22(4):4799–4816, Feb 2014.

[6] G. Bao and D. C. Dobson. On the scattering by a biperiodic structure. *Proceedings of the American Mathematical Society*, 128(9):pp. 2715–2723, 2000.

[7] G. Bao, D. C. Dobson, and J. A. Cox. Mathematical studies in rigorous grating theory. *J. Opt. Soc. Am. A*, 12(5):1029–1042, May 1995.

[8] G. Bao and H. Yang. A least-squares finite element analysis for diffraction problems. *SIAM Journal on Numerical Analysis*, 37(2):665–682, 1999.

[9] A. Barnett and L. Greengard. A new integral representation for quasi-periodic fields and its application to two-dimensional band structure calculations. *Journal of Computational Physics*, 229(19):6898 – 6914, 2010.

[10] A. Barnett and L. Greengard. A new integral representation for quasi-periodic scattering problems in two dimensions. *BIT Numerical Mathematics*, 51(1):67–90, 2011.

[11] A.-S. Bonnet-Bendhia and F. Starling. Guided waves by electromagnetic gratings and non-uniqueness examples for the diffraction problem. *Mathematical Methods in the Applied Sciences*, 17(5):305–338, 1994.

[12] J. Bremer, V. Rokhlin, and I. Sammis. Universal quadratures for boundary integral equations on two-dimensional domains with corners. *J. Comput. Phys.*, 229:8259–8280, 2010.

[13] O. P. Bruno and B. Delourme. Rapidly convergent two-dimensional quasi-periodic Green function throughout the spectrum—including Wood anomalies. *J. Comput. Phys.*, 262:262–290, 2014.

[14] O. P. Bruno and M. C. Haslam. Efficient high-order evaluation of scattering by periodic surfaces: deep gratings, high frequencies, and glancing incidences. *J. Opt. Soc. Am. A*, 26(3):658–668, 2009.

[15] O. P. Bruno and F. Reitich. Numerical solution of diffraction problems: a method of variation of boundaries. *J. Opt. Soc. Am. A*, 10(6):1168–1175, Jun 1993.

[16] Y. Chen, J. S. Hesthaven, Y. Maday, J. Rodriguez, and X. Zhu. Certified reduced basis method for electromagnetic scattering and radar cross section estimation. *Comput. Method Appl. M.*, 233:92–108, 2012.

[17] H. Cheng, C. W. Y., Z. Gimbutas, L. Greengard, J. Huang, V. Rokhlin, N. Yarvin, and J. Zhao. Remarks on the implementation of the wideband FMM for the Helmholtz equation in two dimensions. *Contemporary Mathematics*, 408:99–110, 2006.

[18] M. H. Cho and A. H. Barnett. Robust fast direct integral equation solver for quasi-periodic scattering problems with a large number of layers, 2014. in press, Opt. Expr.

[19] D. Colton and R. Kress. *Integral Equation Methods in Scattering Theory.* Wiley-Interscience, New York, 1983.

[20] D. Colton and R. Kress. *Inverse Acoustic and Electromagnetic Scattering Theory, Applied Mathematical Sciences 93.* Springer-Verlag, Berlin, 1998.

[21] D. C. Dobson. Optimal design of periodic antireflective structures for the Helmholtz equation. *Euro. J. Appl. Math.*, 4:321–340, 1993.

[22] Z. Gimbutas and L. Greengard. Fast multi-particle scattering: A hybrid solver for the Maxwell equations in microstructured materials. *J. Comput. Phys.*, 232:22–32, 2013.

[23] K. L. Greengard, L. Ho and J.-Y. Lee. A fast direct solver for scattering from periodic structures with multiple material interfaces in two dimensions. *J. Comput. Phys.*, 258:738–751, 2014.

[24] L. Greengard and V. Rokhlin. A fast algorithm for particle simulations. *J. Comput. Phys.*, 73(2):325–348, 1987.

[25] J. Helsing and R. Ojala. Corner singularities for elliptic problems: Integral equations, graded meshes, quadrature, and compressed inverse preconditioning. *Journal of Computational Physics*, 227(20):8820 – 8840, 2008.

[26] H. Holter and H. Steyskal. Some experiences from fdtd analysis of infinite and finite multi-octave phased arrays. *Antennas and Propagation, IEEE Transactions on*, 50(12):1725–1731, Dec 2002.

[27] R. Kress. *Linear Integral Equations*. Springer, New York, 1999.

[28] R. Kress and G. F. Roach. Transmission problems for the helmholtz equation. *Journal of Mathematical Physics*, 19(6):1433–1437, 1978.

[29] A. Krishnan, S. Das, S. R. Krishna, and M. Z. A. Khan. Multilayer nanoparticle arrays for broad spectrum absorption enhancement in thin film solar cells. *Opt. Express*, 22(S3):A800–A811, May 2014.

[30] H. Kurkcu and F. Reitich. Stable and efficient evaluation of periodized Green's functions for the Helmholtz equation at high frequencies. *J. Comput. Phys.*, 228:75–95, 2009.

[31] A. A. Lacis, L. D. Travis, and M. I. Mishchenko. *Scattering, Absorption, and Emission of Light by Small Particles*. Cambridge University Press, 2002.

[32] J. Lai, M. Kobayashi, and L. Greengard. A fast solver for multi-particle scattering in a layered medium. *Opt. Express*, 22(17):20481–20499, Aug 2014.

[33] C. Linton and I. Thompson. Resonant effects in scattering by periodic arrays. *Wave Motion*, 44(3):165 – 175, 2007.

[34] C. M. Linton. The Green's function for the two-dimensional Helmholtz equation in periodic domains. *J. Eng. Math.*, 33:377–402, 1998.

[35] A. Marandi, F. Afshinmanesh, and P. P. M. So. Design of a highly focused photonic crystal lens using boolean particle swarm optimization. In *Lasers and Electro-Optics Society, 2007. LEOS 2007. The 20th Annual Meeting of the IEEE*, pages 931–932, 2007.

[36] R. Meisels and F. Kuchar. Density-of-states and wave propagation in two-dimensional photonic crystals with positional disorder. *J. Opt. A*, 9:S396–S402, 2007.

[37] R. Model, A. Rathsfeld, H. Gross, M. Wurm, and B. Bodermann. A scatterometry inverse problem in optical mask metrology. *J. Phys.: Conf. Ser.*, 135:012071, 2008.

[38] M. G. Moharam and T. G. Gaylord. Rigorous coupled-wave analysis of planar-grating diffraction. *J. Opt. Soc. Am.*, 71:811–818, 1981.

[39] C. Müller. *Foundations of the Mathematical Theory of Electromagnetic Waves*. Springer Verlag, 1969.

[40] F. W. J. Olver, D. W. Lozier, R. F. Boisvert, and C. W. Clark. *NIST Handbook of Mathematical Functions*. Cambridge University Press, New York, 2010.

[41] R. Petit. *Electromagnetic Theory of Gratings, Topics in Current Physics*, volume 22. Springer, Heidelberg, 1980.

[42] V. Rokhlin. Solution of acoustic scattering problems by means of second kind integral equations. *Wave Motion*, 5:257–272, 1983.

[43] V. Rokhlin. Rapid solution of integral equations of scattering theory in two dimensions. *J. Comput. Phys.*, 86:414–439, 1990.

[44] R. Santbergen, H. Tan, M. Zemam, and A. H. M. Smets. Enhancing the driving field for plasmonic nanoparticles in thin-film solar cells. *Opt. Expr.*, 22(S4):A1023–A1028, 2014.